Mammalian RNase H2 removes ribonucleotides from DNA to maintain genome integrity

Bjoern Hiller,[1] Martin Achleitner,[1] Silke Glage,[2] Ronald Naumann,[3] Rayk Behrendt,[1] and Axel Roers[1]

[1]Institute for Immunology, Medical Faculty Carl Gustav Carus, University of Technology Dresden, 01307 Dresden, Germany
[2]Institute for Laboratory Animal Science, Hannover Medical School, 30625 Hannover, Germany
[3]Max Planck Institute of Molecular Cell Biology and Genetics, 01307 Dresden, Germany

The Journal of Experimental Medicine

Ribonucleases H (RNases H) are endonucleases which cleave the RNA moiety of RNA/DNA hybrids. Their function in mammalian cells is incompletely understood. RNase H2 mutations cause Aicardi-Goutières syndrome, an inflammatory condition clinically overlapping with lupus erythematosus. We show that RNase H2 is essential in mouse embryonic development. RNase H2–deficient cells proliferated slower than control cells and accumulated in G2/M phase due to chronic activation of a DNA damage response associated with an increased frequency of single-strand breaks, increased histone H2AX phosphorylation, and induction of p53 target genes, most prominently the cyclin-dependent kinase inhibitor 1 encoding cell cycle inhibitor p21. RNase H2–deficient cells featured an increased genomic ribonucleotide load, suggesting that unrepaired ribonucleotides trigger the DNA damage response in these cells. Collectively, we show that RNase H2 is essential to remove ribonucleotides from the mammalian genome to prevent DNA damage.

CORRESPONDENCE
Axel Roers:
axel.roers@tu-dresden.de

Abbreviations used: AGS, Aicardi-Goutières syndrome; ES, embryonic stem; *KOF*, *knockout first*; RNase H, ribonuclease H; topo I, topoisomerase I; TREX1, three prime repair exonuclease 1.

Because of the reactive 2′ hydroxyl group on the ribose ring, ribonucleotides contained in DNA pose a threat to genome stability (Nick McElhinny et al., 2010). High numbers of ribonucleotides were shown to be misincorporated into yeast DNA during replication because ribonucleotide exclusion of replicative polymerases is not absolute (Nick McElhinny et al., 2010). Other sources of ribonucleotides in DNA are Okazaki fragment RNA primers or RNA/DNA hybrids which arise from base pairing of nascent RNA transcripts with their template (Helmrich et al., 2011; Wahba et al., 2011). Ribonuclease H (RNase H) endonuclease activity is defined by specific cleavage of the RNA component of RNA/DNA hybrids (Cerritelli and Crouch, 2009). RNase H2, which accounts for most of the RNase H activity in mammalian cells, recognizes single ribonucleotides in DNA (Cerritelli and Crouch, 2009), suggesting a role in the repair of misincorporated single ribonucleotides in genomic DNA. A PCNA–RNase H2 complex was proposed to scan the genome for ribonucleotides (Bubeck et al., 2011). In addition, RNase H2 may contribute to the removal of Okazaki fragment RNA primers (Turchi et al., 1994). Yeast deficient for RNase H2 was found to display increased genomic ribonucleotide content (Nick McElhinny et al., 2010). Although this phenotype was not associated with reduced proliferation, phosphorylation of Rad53 checkpoint kinase, an accumulation of mutant cells in S phase, and increased sensitivity to replicative stress were observed (Nick McElhinny et al., 2010; Lazzaro et al., 2012). Concomitant abrogation of RNase H1 and 2 in yeast demonstrated that also RNase H1 contributes to ribonucleotide removal (Lazzaro et al., 2012). RNase H–deficient yeast can replicate their ribonucleotide-containing genomes by means of postreplication repair pathways (Lazzaro et al., 2012). RNase H2 deficiency in yeast was demonstrated to result in a mutator phenotype (Nick McElhinny et al., 2010), suggesting that ribonucleotides in DNA are mutagenic if not repaired by RNase H2. In the absence of RNase

R. Behrendt and A. Roers contributed equally to this paper.

The Rockefeller University Press $30.00
J. Exp. Med. 2012 Vol. 209 No. 8 1419-1426
www.jem.org/cgi/doi/10.1084/jem.20120876

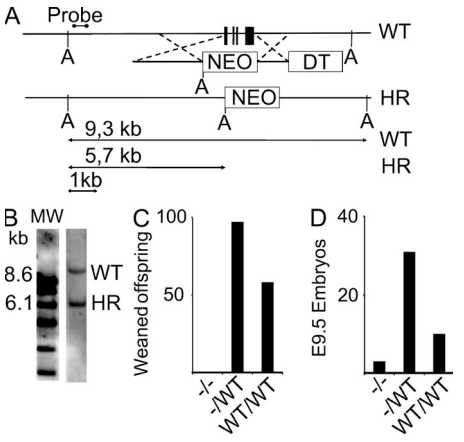

Figure 1. *Rnaseh2c*$^{-/-}$ mice die in utero around day E9.5. (A) Targeting strategy for the generation of *Rnaseh2c*$^{-/-}$ mice. Probe, position of the probe for Southern blot analysis. A, ApaLI cleavage site; HR, homologous recombination; DT, diphtheria toxin; NEO, neomycin/G418 resistance cassette. (B) Southern blot of a targeted ES cell clone. (C) Weaned offspring from heterozygous (*Rnaseh2c*$^{-/WT}$) breedings. (D) Embryos from heterozygous (*Rnaseh2c*$^{-/WT}$) breedings at E9.5.

H2, topoisomerase I (topo I) processes misincorporated ribonucleotides and is responsible for part of the increased mutation rate (Kim et al., 2011).

Mutations in RNase H2 cause Aicardi-Goutières syndrome (AGS), a pediatric inflammatory disorder resembling intrauterine viral infection (Crow et al., 2006b). The condition shows clinical overlap with systemic lupus erythematosus (SLE) and, like SLE, is characterized by an uncontrolled type I IFN response. AGS is also caused by mutations in *TREX1* (*three prime repair exonuclease 1*; Crow et al., 2006a) and *SAMHD1* (Rice et al., 2009) encoding an intracellular 3′-5′ exonuclease and a deoxynucleoside triphosphate triphosphohydrolase, respectively. Mutations of Trex1 are associated with human lupus (Lee-Kirsch et al., 2007), and Trex1 deficiency results in type I IFN–dependent multi-organ inflammation in mice (Morita et al., 2004; Stetson et al., 2008; Gall et al., 2012). This led to a concept of autoimmunity caused by defective degradation of intracellular nucleic acids and their sensing by innate receptors. In this study, we describe that loss of RNase H2 results in increased numbers of ribonucleotides in genomic DNA, spontaneous DNA breaks, and activation of a DNA damage response in mouse cells.

RESULTS AND DISCUSSION

Early embryonic lethality in Rnaseh2c$^{-/-}$ mice

All three subunits of yeast and human RNase H2 are required for enzymatic activity in vitro (Cerritelli and Crouch, 2009) and mutations in any of the three human subunits give rise to AGS. Biallelic null mutations have not been described for any of the three *Rnaseh2* genes and presumably result in early lethality. We generated *Rnaseh2c*$^{-/-}$ mice carrying a deletion of the entire coding region (Fig. 1), likely resulting in complete loss of RNase H2 activity. Homozygous embryos were small at embryonic day 9.5 (E9.5) and were not detected at later time points (not depicted), whereas heterozygous neonates were obtained in expected numbers (Fig. 1). Embryos with presumably complete abrogation of RNase H2 activity were also generated by crossing a conditional *Rnaseh2b* mouse line (see

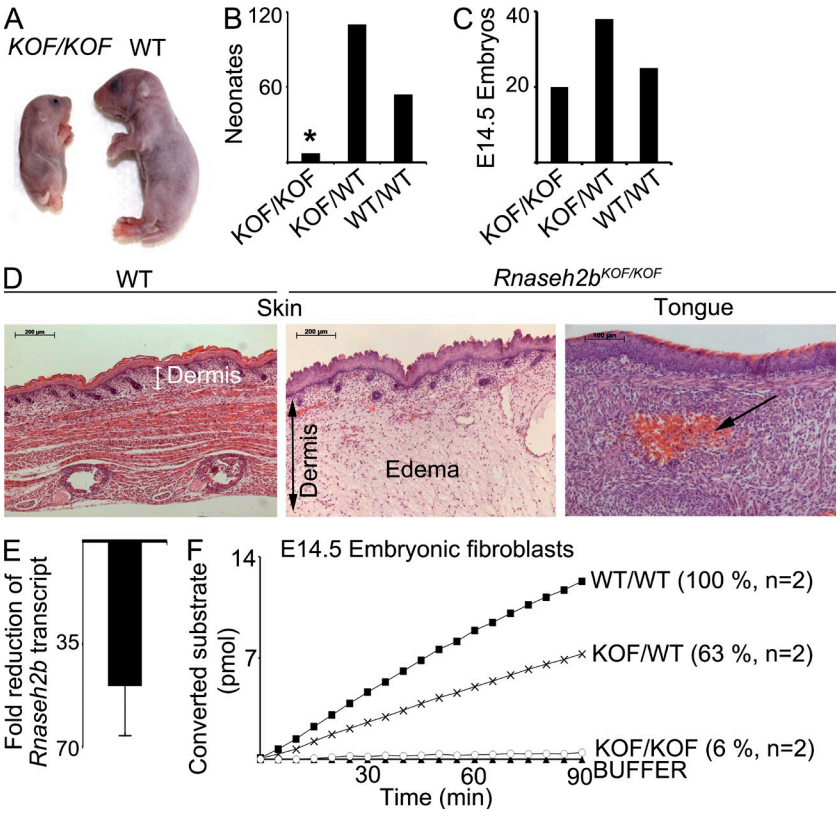

Figure 2. Phenotype of *Rnaseh2b*^{KOF} mice with low levels of residual RNase H2 activity. (A) Control and stillborn homozygous *Rnaseh2b*$^{KOF/KOF}$ neonate. (B) Neonates from heterozygous (*Rnaseh2b*$^{KOF/WT}$) breedings. *, all homozygous neonates were dead upon first inspection. (C) E14.5 embryos from heterozygous (*Rnaseh2b*$^{KOF/WT}$) breedings. (D) Histology of E14.5 *Rnaseh2b*$^{KOF/KOF}$ embryos and littermate controls. Left and middle, H&E-stained section of E14.5 *Rnaseh2b*$^{KOF/KOF}$ and control skin. Note massive edema in mutant skin. Right, H&E-stained section of E14.5 *Rnaseh2b*$^{KOF/KOF}$ tongue. Note the extravasated erythrocytes (arrow) in the muscle tissue. Similar bleedings were detected in numerous tissues of most embryos. (E) Quantification of WT *RNaseh2b* transcripts in fibroblasts from *Rnaseh2b*$^{KOF/KOF}$ and control E14.5 embryos. Mean ± SD of three pairwise comparisons are displayed. (F) RNase H2 activity in E14.5 fibroblasts. Cleavage of an 18-bp dsDNA substrate containing a single ribonucleotide was measured and activity was calculated from the slope of the graphs (means, represented as percentage of WT).

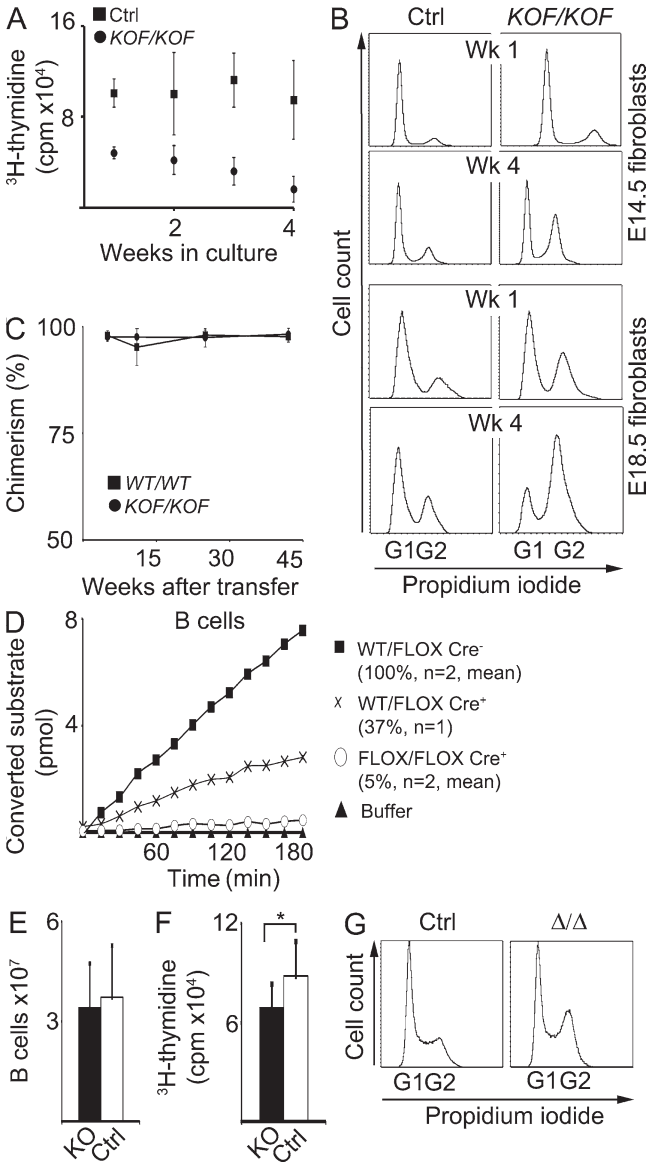

Figure 3. RNase H2–deficient cells show impaired proliferation and accumulate in G2/M. (A) ^{3}H-thymidine incorporation by E14.5 *Rnaseh2b*$^{KOF/KOF}$ (KOF) versus *Rnaseh2b*$^{KOF/WT}$ or *RnaseH2b*$^{WT/WT}$ control (Ctrl) fibroblasts. (B) DNA content analysis. Fibroblasts from E14.5 *Rnaseh2b*$^{KOF/KOF}$ ($n = 10$) or control (WT or heterozygous, $n = 56$) embryos as well as fibroblasts from E18.5 *Rnaseh2b*$^{KOF/KOF}$ ($n = 2$) or control (WT or heterozygous, $n = 5$) embryos were analyzed 1 or 4 wk after initiation of the cultures. One representative result is displayed. (C) Lethally irradiated recipients were transplanted with 4×10^6 fetal liver cells from E14.5 *Rnaseh2b*$^{KOF/KOF}$ ($n = 3$) or WT embryos ($n = 3$). Chimerism was quantified by detection of the congenic CD45.1/2 marker on CD11c$^+$Gr1$^+$ neutrophilic granulocytes. (D) RNase H2 activity in sorted splenic B220$^+$CD19$^+$ B cells from *Rnaseh2b*$^{FLOX/FLOX}$ *CD19-Cre*$^+$ mice ($n = 2$) and controls (*WT/FLOX* Cre$^+$, $n = 1$; and *WT/FLOX* Cre-negative, $n = 2$). Purity of the sorted B cells was 96.5–97.7%. (E) Numbers of splenic CD19$^+$B220$^+$ B cells in adult *Rnaseh2b*$^{FLOX/FLOX}$ *CD19-Cre*$^+$ (KO, $n = 6$) and controls (Ctrl, FLOX/FLOX Cre$^-$ or FLOX/WT CRE$^+$, $n = 6$). (F) ^{3}H-thymidine incorporation by *Rnaseh2b*$^{FLOX/FLOX}$ *CD19-Cre*$^+$ ($n = 9$) and control (Ctrl, FLOX/FLOX Cre$^-$ or FLOX/WT CRE$^+$, $n = 9$) B cells. Total splenocytes were analyzed after 3 d of culture in the presence of LPS. *, $P < 0.05$ (two-tailed Student's t test). (G) DNA content analysis. Splenic B cells from *Rnaseh2b*$^{FLOX/FLOX}$ *CD19-Cre*$^+$ (Δ/Δ, $n = 6$) and control mice (Ctrl, FLOX/FLOX Cre$^-$ or FLOX/WT CRE$^+$, $n = 6$) were analyzed after 3 d in vitro LPS stimulation. One representative result is displayed. Error bars indicate ±SD in all graphs.

Materials and methods) to a general *Cre*-deleter strain (Lallemand et al., 1998) and displayed lethality similar to *Rnaseh2c*$^{-/-}$ embryos (unpublished data). Thus, RNase H2 activity is essential in mouse embryonic development.

Perinatal lethality in mice with reduced RNase H2B expression

In addition to *Rnaseh2c*$^{-/-}$ mice, a mouse line carrying a gene trap cassette inserted into *Rnaseh2b* intron 4/5 (*Rnaseh2b knockout first* [*KOF*] mice) was analyzed. The gene trap cassette is expected to be spliced to exon 4 and terminate translation (Testa et al., 2004). Mice homozygous for the *KOF* allele were underrepresented at birth (Fig. 2), were significantly smaller compared with littermate controls, and died perinatally (Fig. 2). Already at E14.5, homozygous embryos were small but present at Mendelian ratios (Fig. 2). Histological analysis revealed proportionally small organs. Many tissues were edematous and displayed extended vessels, as well as bleedings, suggesting defects in vessel wall architecture (Fig. 2). FACS analysis of E18.5 liver and thymus revealed a massive reduction of cellularity (unpublished data). Because the gene trap cassette may allow normal mRNA splicing to some degree, we analyzed E14.5 fetal liver (not depicted) or fibroblasts for residual normal transcripts and found them reduced to a small percentage compared with control levels (Fig. 2). Correspondingly, RNase H2 activity was reduced to 6% of normal values in extracts from E14.5 fibroblasts (Fig. 2) and liver (not depicted). Fibroblasts from two additional *Rnaseh2b*$^{KOF/KOF}$ and control embryos yielded similar results (unpublished data). Thus, the *Rnaseh2b*^{KOF} mutation represents a hypomorphic allele with low residual enzyme activity.

RNase H2 deficiency impairs proliferation and triggers a DNA damage response

Rnaseh2b$^{KOF/KOF}$ E14.5 fibroblasts proliferated slower than control cultures (Fig. 3) and this defect became more pronounced with increasing passage numbers. Reduced proliferation of these cultures was not a result of enhanced apoptosis because fractions of propidium iodide$^+$ and annexin V$^+$ cells were not increased (unpublished data). DNA content analysis revealed mildly increased numbers of cells in S and G2/M phase in (asynchronous) 1-wk-old mutant versus control cultures (Fig. 3). The fraction of mutant cells in G2/M markedly increased with the duration of the culture. In E18.5 fibroblasts, the accumulation of cells in G2/M was striking already after 1 wk of culture, and 4-wk-old E18.5 fibroblast cultures contained 70–80% of cells in G2/M (Fig. 3). This finding suggested that the problem caused by RNase H2 deficiency exacerbates with increasing numbers of divisions.

To test the proliferative capacity of mutant hematopoietic cells, we transferred E14.5 *Rnaseh2b*$^{KOF/KOF}$ liver cells into lethally irradiated recipients. Transfer of a standard radioprotective

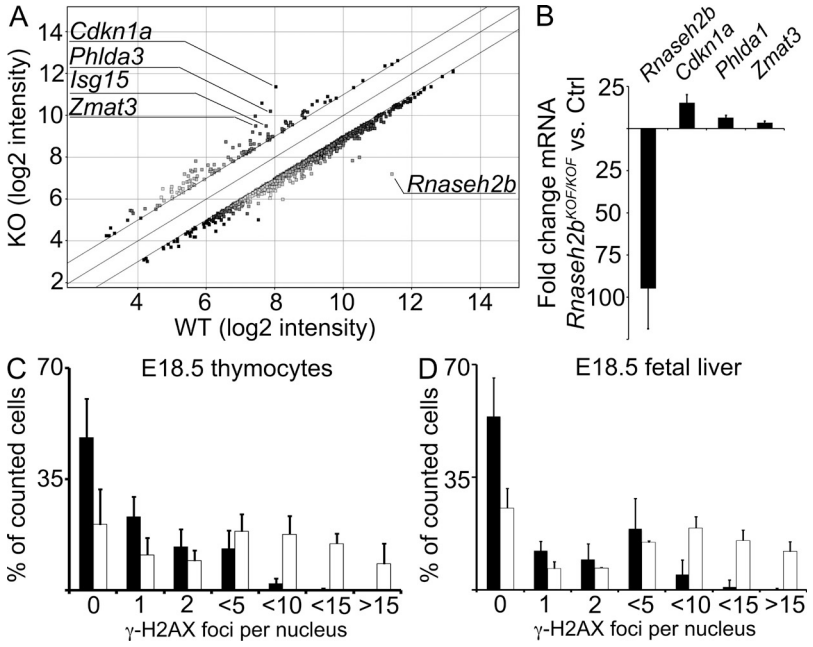

Figure 4. Enhanced transcription of p53-inducible genes and DNA damage in RNase H2B–deficient cells. (A) Comparison of gene expression profiles in liver cells from *Rnaseh2b*$^{KOF/KOF}$ and WT control E14.5 embryos (n = 3 both groups) by microarray analysis. The graph shows genes with more than twofold difference in transcript levels between the groups. (B) Validation of mRNA levels in E14.5 fetal liver by qRT-PCR for the *Rnaseh2b* and three p53-inducible genes. Results of three pairwise comparisons of *Rnaseh2b*$^{KOF/KOF}$ and WT control samples are displayed. (C and D) *Rnaseh2b*$^{KOF/KOF}$ (n = 6, white bars) or control (WT/WT or KOF/WT, n = 11, black bars) E18.5 thymocytes (C) and *Rnaseh2b*$^{KOF/KOF}$ (n = 4, white bars) or control (WT/WT or KOF/WT, n = 9, black bars) E18.5 liver cells (D) were immunostained for phosphorylated histone H2AX (γ-H2AX). 400 nuclei per individual thymus or liver were evaluated in a blinded fashion. Error bars indicate ±SD in all graphs.

number of liver cells did not result in stable chimerism (unpublished data), whereas transfer of 4 × 10^6 *Rnaseh2b*$^{KOF/KOF}$ cells (20× radioprotective dose) resulted in long-term rescue with chimerism close to 100% (Fig. 3). In these chimeric animals, leukocyte numbers tended to be lower compared with recipients of control cells but were in the normal range (unpublished data). Red blood cell counts were not different between the groups (unpublished data). Thus, reduced RNase H2 activity impairs cell cycle progression but does not preclude substantial proliferative expansion of hematopoietic cells.

To bypass lethality of complete RNase H2 deficiency, we generated *Rnaseh2b*^{FLOX} mice by Flpe-mediated deletion of the gene trap cassette of the *Rnaseh2b*^{KOF} allele to create conditional *Rnaseh2b* knockout mice. *Rnaseh2b*^{FLOX} mice were crossed to *CD19-Cre* mice (Rickert et al., 1997) for B cell–specific gene inactivation. (Cre-mediated deletion of *exon5* introduces a frame shift.) B cell numbers of *Rnaseh2b*$^{FLOX/FLOX}$*CD19-Cre*$^+$ mice were normal in spleen (Fig. 3). Overgrowth of the B cell compartment by cells that had escaped Cre-mediated gene inactivation was excluded by analysis of protein extracts from sorted B cells for RNase H2 activity (Fig. 3). *Rnaseh2b*$^{FLOX/FLOX}$ *CD19-Cre*$^+$ B cells featured a reduction of activity to 5.6 ± 2.1% (n = 2). Post-sort reanalysis determined the purity of the sorted B cells to range from 96.5–97.7% (unpublished data), indicating that about half of the residual RNase H2 activity was accounted for by contaminating non–B cells. Thus, most *Rnaseh2b*$^{FLOX/FLOX}$ *CD19-Cre*$^+$ B cells were completely devoid of RNase H2 activity. CD19-Cre–driven recombination commences in B cell development and is ongoing at the pre–B cell stage (Rickert et al., 1997). Our findings indicate that complete deficiency for RNase H2 in precursor B cells does not preclude a limited number of divisions required to fill up peripheral B cell compartments. Proliferation of LPS-stimulated *Rnaseh2b*$^{FLOX/FLOX}$ *CD19-Cre*$^+$ B cell cultures was reduced to 80% compared with controls (Fig. 3) with a moderate accumulation of mutant B cells in G2/M (Fig. 3). Collectively, RNase H2 deficiency impairs proliferation but does not preclude considerable proliferative expansion in vivo.

Microarray-based gene expression profiling of *Rnaseh2b*$^{KOF/KOF}$ versus WT E14.5 liver cells revealed a striking up-regulation of p53-inducible genes in *Rnaseh2b*$^{KOF/KOF}$ versus control E14.5 liver cells (GEO database accession no. GSE36687). The top seven genes up-regulated in mutant versus control included four p53 target genes, with *Cdkn1a*, encoding cyclin-dependent kinase inhibitor 1 (p21), being the gene with the most prominent up-regulation of all differentially regulated genes (Fig. 4). Enhanced transcription of these genes was validated by quantitative (q) RT-PCR (Fig. 4). A large number of genes involved in mitosis showed reduced transcript levels in the mutant samples (unpublished data). Our results suggested that RNase H2–deficient cells feature cell cycle arrest mediated via p53-induced p21 expression. To detect DNA damage that triggered p53 activation, we stained E18.5 *Rnaseh2b*$^{KOF/KOF}$ thymocytes and liver cells for phosphorylated histone H2AX (γ-H2AX), which is induced in chromatin flanking double-strand breaks, and found significantly increased numbers of γ-H2AX foci per nucleus in mutant cells (Fig. 4). In addition to enhanced H2AX phosphorylation, we detected increased numbers of spontaneous single-strand breaks in DNA from embryos with complete RNase H2 deficiency (see next section). Collectively, our data indicate that RNase H2–deficient cells spontaneously activate a DNA damage response.

Similar to our findings in RNase H2–deficient cells, compromised proliferation, spontaneous DNA damage, and chronic checkpoint activation were also reported for a *Trex1*$^{-/-}$ mouse embryonic fibroblast line and fibroblasts from AGS patients with Trex1 mutations by Yang et al. (2007). *Trex1*$^{-/-}$ cells featured p21 expression, a defective G2/M

cell cycle checkpoint, and a block in G1/S transition (Yang et al., 2007). These findings, however, were not reproduced by Stetson et al. (2008), who did not find impaired proliferation or evidence of a DNA damage response in primary embryonic fibroblasts from *Trex1*$^{-/-}$ mice. In our primary RNase H2–deficient cells, the G2/M checkpoint seemed to be intact and may be responsible for the observed p21-mediated arrest. Although p21 is well known to block G1/S transition, p21 was also shown to arrest cells in G2 by inhibition of CDK1 (Bunz et al., 1998).

RNase H2 deficiency results in an increased genomic ribonucleotide load

DNA from RNase H2–deficient yeast displays enhanced sensitivity to alkaline hydrolysis, indicating an increased genomic ribonucleotide content (Nick McElhinny et al., 2010). To test whether RNase H2 deficiency in mammalian cells is associated with increased numbers of ribonucleotides in DNA, we used bacterial RNase HII to introduce nicks into chromosomal DNA at positions of ribonucleotides. DNA was purified using standard procedures and contains few double-strand breaks as a result of shear stress, resulting in large fragments in the range of several hundred kilobases. Nicks were detected by DNA polymerase I–dependent nick translation incorporating label into the DNA, which was then run on an agarose gel and visualized by autoradiography. Assuming equal mean length of the single strand polymerized de novo by pol I in mutant versus WT DNA and loading of equal amounts of DNA per lane (determined photometrically for each sample), incorporation of label correlates with numbers of nicks present in the genomic DNA. We found massive RNase HII–dependent incorporation of label into DNA from RNase H2–deficient (*rnh201Δ*; Nick McElhinny et al., 2010) but not WT (Fig. 5) yeast, confirming that the increased sensitivity of mutant yeast DNA to alkaline hydrolysis (Nick McElhinny et al., 2010) was caused by the presence of increased numbers of ribonucleotides. Likewise, DNA from E9.5 *Rnaseh2b*$^{\Delta/\Delta}$ (Fig. 5) and Rnaseh2c$^{-/-}$ (Fig. 5) embryos displayed RNase HII–dependent incorporation of label, indicating increased numbers of ribonucleotides. Similar results were obtained for two additional *Rnaseh2b*$^{\Delta/\Delta}$ and four additional Rnaseh2c$^{-/-}$ embryos (unpublished data). Importantly, for all 11 mutant embryos tested, the assay consistently revealed increased incorporation of label compared with DNA from control embryos also in those samples without pretreatment with bacterial RNase HII (Fig. 5 and not depicted), demonstrating that DNA from RNase H2–deficient cells contains higher numbers of spontaneous single-strand breaks as compared with control DNA. The increased genomic ribonucleotide load in RNase H2–deficient mouse cells demonstrates that, like the yeast enzyme, mammalian RNase H2 also functions to remove ribonucleotides from genomic DNA. Our assay did not discriminate whether the accumulating ribonucleotides in RNase H2–deficient DNA represented single nucleotides misincorporated during replication, incompletely removed Okazaki primers, or R-loop structures. Because RNase H1—which cannot cleave at single ribonucleotides but requires at least four subsequent ribonucleotides (Cerritelli and Crouch, 2009)—did not compensate for the loss of RNase H2, it appears likely that the accumulating ribonucleotides in RNase H2–deficient mouse cells are single nucleotides misincorporated by DNA polymerases.

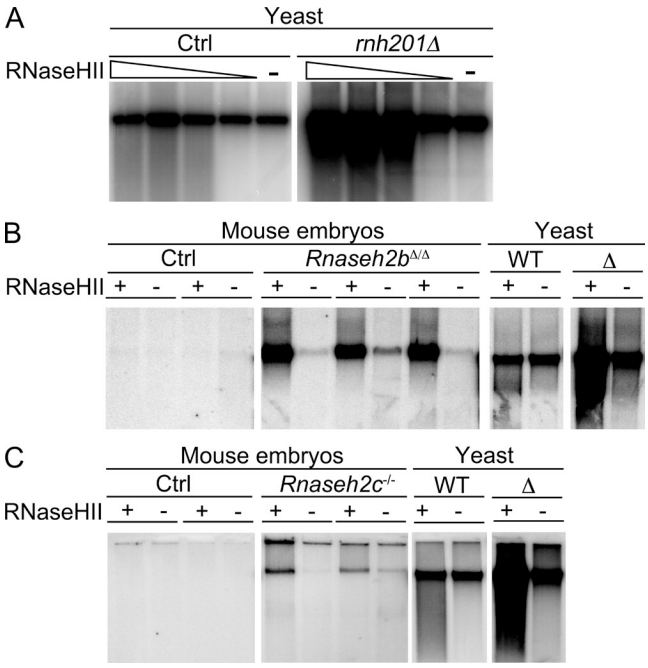

Figure 5. Increased numbers of ribonucleotides in genomic DNA of RNase H2–deficient embryos. Large chromosomal fragments obtained by standard DNA purification were nicked by bacterial RNase HII at ribonucleotide positions, followed by DNA polymerase I–dependent nick translation in the presence of ^{32}P-dCTP. Labeled DNA was run on a 1% agarose gel (focusing the large chromosomal fragments [several hundred kilobases] in a distinct band) and visualized by autoradiography. Control samples were not digested with RNase HII to detect background single strand breaks. (A) DNA from RNase H2–deficient (*rnh201Δ*) or control yeast (Ctrl) was digested with increasing amounts (1–10 mU/µl) of RNase HII or subjected to nick translation without RNase HII pretreatment. (B) 200 ng DNA from WT (Ctrl) and *Rnaseh2b*$^{\Delta/\Delta}$ embryos (obtained by crossing *Rnaseh2b*^{FLOX} mice with *PGK-Cre* mice) was digested with 10 mU/µl RNase HII before nick translation. Negative control samples from each embryo were not pretreated with RNase HII. DNA from RNase H2–proficient (WT) and –deficient (Δ) yeast served as controls. (C) Experiment as in B performed with DNA from Rnaseh2c$^{-/-}$ and WT control embryos. All panels in A, B, and C originate from the same exposure of one single gel each.

Our data strongly suggest that defective ribonucleotide repair triggers the spontaneous damage response of mutant cells. Breaks in RNase H2–deficient DNA may in part reflect lower chemical stability of the ribonucleotide-containing genome. In addition, topoisomerase-mediated cleavage of ribonucleotide-containing DNA could explain the higher frequency of strand breaks in RNase H2–deficient cells. Topo I was reported to cleave double-stranded DNA substrates containing single ribonucleotides resulting in a single-strand break with one 2′,3′-cyclic phosphate end (Sekiguchi and Shuman., 1997; Kim et al., 2011). The damage response could also

be a result of collisions of widespread topo I cleavage complexes with replication forks resulting in replication-mediated double-strand breaks (Furuta et al., 2003) or to compromised resolution of RNA/DNA hybrids arising from spontaneous errors of RNA biogenesis. Such R-loop structures represent substrates for RNase H activity in yeast and their persistence was demonstrated to predispose to double-strand break formation (Wahba et al., 2011; Stirling et al., 2012).

The relevance of the spontaneous damage response we found in RNase H2–deficient mouse cells for the pathogenesis of AGS is unclear. Genome instability and increased incidence of neoplastic disease were not reported in RNase H2–associated AGS. Embryonic lethality, spontaneous DNA damage response, and increased genomic ribonucleotide load were also described in another study of RNase H2 mutant mice (Reijns et al., 2012).

Lethal phenotype of RNase H2–deficient embryos is independent of type I IFN

Deficiency for Trex1 causes AGS and/or Lupus, both of which are inflammatory conditions characterized by a chronic type I IFN response (Crow, 2011). *Trex1*$^{-/-}$ mice develop type I IFN and lymphocyte-dependent autoimmune multiorgan inflammation (Morita et al., 2004; Stetson et al., 2008; Gall et al., 2012). The IFN response initiated in utero before E14 (Gall et al., 2012). Similar to *Trex1* mutations, defects in RNase H2 also cause AGS. We therefore expected spontaneous IFN-mediated pathology in our RNase H2–deficient mice. However, crossing the *RNaseh2b*^{KOF} strain to type I IFN receptor-deficient (*IFNAR1*$^{-/-}$) mice (Müller et al., 1994) did not result in a rescue of perinatal lethality (unpublished data). Both *RNaseh2b*$^{KOF/KOF}$ *IFNAR1*$^{-/-}$ E17.5 embryos obtained so far featured similar growth retardation as *RNaseh2b*$^{KOF/KOF}$ animals with intact type I IFN system and living *RNaseh2b*$^{KOF/KOF}$ *IFNAR1*$^{-/-}$ neonates were not found. In accordance with this finding, gene expression profiling of *RNaseh2b*$^{KOF/KOF}$ E14.5 liver cells (Fig. 4) did not reveal a clear signature of up-regulated IFN-responsive genes (unpublished data). Few IFN-inducible genes were found up-regulated; however, several of these are also responsive to p53 and may not reflect type I IFN effects in our mice. Inflammatory changes were not found upon detailed histological analysis of serial sections of whole mount E14.5, E18.5, or stillborn *RNaseh2b*$^{KOF/KOF}$ embryos (unpublished data). A cross to *RAG1*$^{-/-}$ mice did not rescue the pathology of *RNaseh2b*$^{KOF/KOF}$ animals (unpublished data), indicating that lymphocytes have no role in the lethal phenotype. We speculate that IFN-mediated autoimmune pathology might commence at later stages of ontogeny in mouse models of less severe or conditional RNase H2 deficiency which bypass early lethality. A milder reduction of RNase H2 activity in AGS patients compared with our mouse models may explain that a DNA damage–related phenotype dominates in the latter but not in RNase H2–associated AGS. Whether a low-level chronic DNA damage response contributes to the pathogenesis of AGS and related human disorders remains an open question.

MATERIALS AND METHODS

Mice. *Rnaseh2c*$^{-/-}$ mice were generated by homologous recombination in JM8.F6 (C57BL/6) cells. For targeted deletion of all four exons of the *Rnaseh2c* gene, upstream and downstream homology regions (1,800 and 900 bp, respectively) were amplified from C57BL/6 genomic DNA (primers: 5′HR up, 5′-GGACTTCTAGATGGTACTTTGCAAGCAGCCCCTGGAGGAGA-3′; 5′HR down, 5′-CGTACCGGATCCGTGATGAGGATTGGACTCAGGGCCTTGGAC-3′; 3′HR up, 5′-TATGGTGTCCTAGGCTTTAGCTAGTCGCAGTCATTAAGCTTCTTTGGTCCACGTGTTCAGAGCGGACCTGG-3′; and 3′HR down, 5′-CCTAATGAATTGGCCTGTAGCTGGTAGTCTATCCATCTCGAGACTCCGCCTCCTGTGCTCTATTGCTTTAGG-3′) and cloned into the vector pBluescript (using restriction sites contained in the primers) to flank a PGK-gb2-neomycin resistance cassette, which had been inserted into the multiple cloning site. For negative selection against random integration of the targeting vector, a diphtheria toxin cassette was inserted downstream of the 3′ homology region. The linearized vector was transfected into embryonic stem (ES) cells and recombinant clones were detected by Southern blot analysis of ApaLI-digested DNA. The probe was amplified from BAC RP23-156A18 (BACPAC Resources Center; primers: H2C probe up, 5′-CTGAAACGAGATGGAGTGACCATGAGGAC-3′; and H2C probe down, 5′-GTCCTAATAGGGACAGGAAATTGCTCTG-3′) and labeled fragments of 9.3 and 5.7 kb in WT and targeted locus, respectively. Positive clones were injected into albino C57BL/6 foster mothers. Chimeric animals were crossed to C57BL/6 mice and offspring was genotyped by PCR (primers: H2c wt forward, 5′-CACAGATCCCTTCTCACCACTTGGA-3′; H2c neo forward, 5′-CTGCTTGCCGAATATCATGGTGGAA-3′; and H2c reverse, 5′-CCGAAGAACAGACCCAAGAGGAGAA-3′) to detect germline transmission of the mutation.

Heterozygous *Rnaseh2b*^{KOF} mice (C57BL/6) were purchased from the International Knockout Mouse consortium and were genotyped by PCR as recommended by the vendor. For generation of the conditional *Rnaseh2b*^{FLOX} mouse line, *Rnaseh2b*^{KOF} mice were bred to the *Flpe*-deleter mouse strain (Rodríguez et al., 2000) and successful deletion of the *frt*-flanked gene trap cassette was demonstrated by PCR. All mouse strains were on the C57BL/6 background. Mice were housed at the Experimental Centre at University of Technology Dresden, Medical Faculty Carl-Gustav Carus, under specific pathogen-free conditions. All procedures were in accordance with institutional guidelines on animal welfare and were approved by the Landesdirektion Dresden.

Cell culture. Upon cesarean section, E14.5 or 18.5 mouse embryos were decapitated and internal organs were removed. Tissue was minced, digested with 1× trypsin (2.5%; Invitrogen) for 15 min at 37°C, and disaggregated by pipetting. The cell suspension was seeded into 10-cm Petri dishes in DME (Gibco) containing 10% fetal bovine serum (Biochrom), 100 U/ml penicillin and 100 µg/ml streptomycin (Biochrom), 1× nonessential amino acids (Biochrom), and 100 µM β-mercaptoethanol (Sigma-Aldrich).

Cell cycle analysis. Embryonic fibroblasts were seeded into a 6-well plate (5×10^5 cells/well) and cultivated for 3 d. Cells were harvested, washed once with PBS, fixed in 70% ice-cold ethanol, and chilled for at least 12 h at −20°C, followed by washing in PBS and resuspension and 10-min incubation at room temperature in 0.5 µg/ml RNase A (Sigma-Aldrich) and 2.5 µg/ml propidium iodide (Sigma-Aldrich). Cells were analyzed on a MACSQuant flow cytometer (Miltenyi Biotec).

^{3}H-thymidine incorporation. Embryonic fibroblasts were seeded into flat-bottom 96-well plates (5×10^3 cells/well) and cultivated for 48 h in complete DME (see Cell culture). 3.7×10^4 Bq ^{3}H-thymidine (HARTMANN ANALYTICS) was added to each well, and after a further 48 h of culture, cells were harvested and washed. Incorporation of ^{3}H-thymidine was determined using a 1450 MicroBeta TriLux scintillation counter (Perkin Elmer).

B cell in vitro stimulation. Total splenocytes were cultivated in 6-well plates at a density of 3×10^5 cells/ml in RPMI 1640 supplemented with 10%

fetal bovine serum (Biochrom) and 100 U/ml penicillin and 100 µg/ml streptomycin, 2 mM L-alanyl-L-glutamine (Biochrom), 10 µM β-mercaptoethanol, and 25 µg/ml lipopolysaccharide from *Salmonella minnesota Re 595* (Sigma-Aldrich). For DNA content analysis, cells were harvested after 3 d. For proliferation assays, 3.7×10^4 Bq ^{3}H-thymidine per well was added after 48 h and the cells were incubated for an additional 24 h, followed by harvesting and quantification of ^{3}H-thymidine incorporation.

Quantitative PCR. Total RNA was isolated using TRIzol (Invitrogen) according to the manufacturer's instructions. For qRT-PCR, RNA was digested with DNaseI (New England Biolabs, Inc.) and purified using the RNeasy Mini kit (QIAGEN). 200 ng–1 µg RNA was reverse transcribed using a poly(dT) primer of the RevertAid H Minus First Strand cDNA Synthesis kit (Thermo Fisher Scientific) according to the manufacturer's recommendations. 1 µl of the cDNA product served as template in the subsequent qRT-PCR using the Maxima SYBR green/ROX qPCR Master Mix (Thermo Fisher Scientific) using 0.6 µM target specific primers, initial denaturation at 95°C for 15 min, 40 cycles of denaturation (15 s at 95°C), annealing (30 s at 58°C), and elongation (30 s at 72°C). Incorporation of SYBR green was analyzed using the Mx3005P QPCR system (Agilent Technologies) and the MxPro QPCR Software. RT-PCR primers were as follows: p21 up, 5′-GCAATCCACAGCGATATCC-3′; p21 down, 5′-CAACTGCTCACTGTCCACGG-3′ (Kanatsu-Shinohara et al., 2010); Zmat3 up, 5′-GAGTCACTCATTCTCGGACTCCGC-3′; Zmat3 down, 5′-GAGCGGGCATTGAAGTAAGGGC-3′; Phlda3 up, 5′-TTCGCCCGCATCAAAGCCGT-3′; Phlda3 down, 5′-AGGGGGCAGCGGAAGTCGAT-3′ (Brady et al., 2011); Rnaseh2b up, 5′-AGGTTTCCAGGGACAAGGAAGAGGA-3′; Rnaseh2b down, 5′-GTCAATGAAGCTGGAGGTTCTGGAAG-3′; β-actin up, 5′-TGACCCAGATCATGTTTGAGACCTTCA-3′; and β-actin down, 5′-GGAGTCCATCACAATGCCTGTGG-3′. Measured transcript levels were normalized to β-actin. All samples were run in triplicate.

Microarray analysis of fetal liver of RNaseH2b KOF mice. Fetal livers of E14.5 embryos were homogenized using the gentleMACS Dissociator (Miltenyi Biotec). RNA was isolated using the acid guanidinium thiocyanate-phenol-chloroform method (Chomczynski and Sacchi, 2006). RNA quality was determined on a Bioanalyzer instrument (Agilent Technologies). The RNA was reverse transcribed, amplified, and biotin labeled using the Message Amp II-Biotin Enhanced kit (Ambion). Hybridization, staining, and scanning of the GeneChip Mouse Genome 430 2.0 microarrays were performed according to the GeneChip Expression Analysis Technical Manual P/N 702232 Rev. 3 (Affymetrix). Microarray data were analyzed using GeneSpring GX software. Deregulated genes of interest were validated by qRT-PCR. All microarray data were deposited in the GEO database (accession no. GSE36687).

Nick translation assay for ribonucleotide content of genomic DNA. 200 ng mouse or yeast genomic DNA (quantified using an ND-1000; Nanodrop Technologies) was digested with 0.5 U *E. coli* RNase HII (New England Biolabs, Inc.) in a total volume of 50 µl and the recommended buffer at 37°C for 2.5 h, precipitated in 0.3 M sodium acetate, pH 5.2, and ethanol. DNA was dissolved in water and nick translation reagents were added to final concentrations of 1× buffer 2 (New England Biolabs, Inc.) and 20 µM unlabeled dATP, dGTP, and dTTP (Thermo Fisher Scientific). 5 U *E. coli* DNA polymerase I (New England Biolabs, Inc.) and 3.7×10^5 Bq ^{32}P-dCTP (Hartmann Analytics) were added, and the reaction volume was adjusted to 20 µl. The reaction was incubated at 16°C for 35 min. Labeled high molecular weight DNA was separated from unincorporated nucleotides by electrophoresis on a 1% TAE agarose gel and visualized by autoradiography (PhosphorImager SI; Molecular Dynamics) of dried gels (GD 2000 Vacuum Gel Dryer system; GE Healthcare).

Generation of chimeric mice. Fetal liver cells were isolated from E14.5 embryos and homogenized by repeated aspiration through an 18G needle followed by aspiration through a 20G needle. Cell numbers were determined without lysis of red blood cells. Lethally irradiated (7 Gy) CD45.1/2 congenic recipient mice were reconstituted with 2.5×10^5 or 4×10^6 total fetal liver cells (1.25 or 20× radioprotective dose, respectively) by retro-orbital intravenous injection. Chimerism was assessed in CD11b$^+$Gr1$^+$ neutrophilic granulocytes by flow cytometry FACSCalibur (BD) at various time points starting at week 4 after transfer.

Staining for phosphorylated histone H2AX (γ-H2AX). Cytospins of 10^5 E18.5 fetal liver or E18.5 fetal thymocytes were washed in Tris-buffered saline (TBS). Cells were fixed in 4% formaldehyde for 30 min at RT and permeabilized in TBS containing 0.25% Triton X-100 for an additional 10 min at room temperature, followed by blocking with 3% bovine serum albumin (Serva) in TBS for at least 1 h at room temperature, incubation with a 1:500 dilution of the anti–γ-H2AX antibody (clone JBW301; Millipore) in blocking buffer, washing, and detection using a 1:1,000 dilution of Alexa Fluor 488 goat anti–mouse IgG (Life Technologies) in blocking buffer. Nuclei were counterstained with DAPI.

Assay for RNase H2 activity. Cell lysates were prepared and assayed for specific cleavage of an 18-bp double-stranded DNA substrate containing a single ribonucleotide in one strand as previously described (Reijns et al., 2011). RNase H2–specific activity was determined by subtracting the cellular activity against a sequence-matched DNA duplex without ribonucleotides. Cell lysate protein concentration was determined and lysates were added to the reaction mix at a final protein concentration of 100 ng/µl for fetal liver and fibroblast lysates. Lysates of B cells contained less protein and were added to reactions to final concentration of 5 ng/µl.

Statistical analysis. Data are shown as means ± SD. Statistical analysis was performed with the Student's *t* test.

The authors thank Martin Reijns and Andrew Jackson for performing enzyme activity assays and for sharing unpublished data. We are grateful to Thomas Kunkel for providing RNase H2–deficient yeast strains, Julia Jarrells and Britta Schilling for microarray analyses, Dora Schreier for ES cell transfection and morula injections, Min-Ae Lee-Kirsch, Werner Müller, Michael Bachmann, Rolf Jessberger, Frank Buchholz, Dragomir Krastev, and Alexander Gerbaulet for advice and discussions, and Christina Hiller and Tobias Häring for expert technical assistance.

This work was supported by the German Research Foundation (Klinische Forschergruppe KFO 249, project TP7, Ro2133/6-1) to A. Roers and "MeDDrive" grants 60.230 and 60.294 of the Medical Faculty Carl Gustav Carus, TU-Dresden, to R. Behrendt.

The authors have no competing financial interest.

Submitted: 24 April 2012
Accepted: 11 June 2012

REFERENCES

Brady, C.A., D. Jiang, S.S. Mello, T.M. Johnson, L.A. Jarvis, M.M. Kozak, D. Kenzelmann Broz, S. Basak, E.J. Park, M.E. McLaughlin, et al. 2011. Distinct p53 transcriptional programs dictate acute DNA-damage responses and tumor suppression. *Cell*. 145:571–583. http://dx.doi.org/10.1016/j.cell.2011.03.035

Bubeck, D., M.A. Reijns, S.C. Graham, K.R. Astell, E.Y. Jones, and A.P. Jackson. 2011. PCNA directs type 2 RNase H activity on DNA replication and repair substrates. *Nucleic Acids Res*. 39:3652–3666. http://dx.doi.org/10.1093/nar/gkq980

Bunz, F., A. Dutriaux, C. Lengauer, T. Waldman, S. Zhou, J.P. Brown, J.M. Sedivy, K.W. Kinzler, and B. Vogelstein. 1998. Requirement for p53 and p21 to sustain G2 arrest after DNA damage. *Science*. 282:1497–1501. http://dx.doi.org/10.1126/science.282.5393.1497

Cerritelli, S.M., and R.J. Crouch. 2009. Ribonuclease H: the enzymes in eukaryotes. *FEBS J.* 276:1494–1505. http://dx.doi.org/10.1111/j.1742-4658.2009.06908.x

Chomczynski, P., and N. Sacchi. 2006. The single-step method of RNA isolation by acid guanidinium thiocyanate-phenol-chloroform extraction: twenty-something years on. *Nat. Protoc.* 1:581–585. http://dx.doi.org/10.1038/nprot.2006.83

Crow, Y.J. 2011. Type I interferonopathies: a novel set of inborn errors of immunity. *Ann. N.Y. Acad. Sci.* 1238:91–98. http://dx.doi.org/10.1111/j.1749-6632.2011.06220.x

Crow, Y.J., B.E. Hayward, R. Parmar, P. Robins, A. Leitch, M. Ali, D.N. Black, H. van Bokhoven, H.G. Brunner, B.C. Hamel, et al. 2006a. Mutations in the gene encoding the 3′-5′ DNA exonuclease TREX1 cause Aicardi-Goutières syndrome at the AGS1 locus. *Nat. Genet.* 38:917–920. http://dx.doi.org/10.1038/ng1845

Crow, Y.J., A. Leitch, B.E. Hayward, A. Garner, R. Parmar, E. Griffith, M. Ali, C. Semple, J. Aicardi, R. Babul-Hirji, et al. 2006b. Mutations in genes encoding ribonuclease H2 subunits cause Aicardi-Goutières syndrome and mimic congenital viral brain infection. *Nat. Genet.* 38:910–916. http://dx.doi.org/10.1038/ng1842

Furuta, T., H. Takemura, Z.Y. Liao, G.J. Aune, C. Redon, O.A. Sedelnikova, D.R. Pilch, E.P. Rogakou, A. Celeste, H.T. Chen, et al. 2003. Phosphorylation of histone H2AX and activation of Mre11, Rad50, and Nbs1 in response to replication-dependent DNA double-strand breaks induced by mammalian DNA topoisomerase I cleavage complexes. *J. Biol. Chem.* 278:20303–20312. http://dx.doi.org/10.1074/jbc.M300198200

Gall, A., P. Treuting, K.B. Elkon, Y.M. Loo, M. Gale Jr., G.N. Barber, and D.B. Stetson. 2012. Autoimmunity initiates in nonhematopoietic cells and progresses via lymphocytes in an interferon-dependent autoimmune disease. *Immunity.* 36:120–131. http://dx.doi.org/10.1016/j.immuni.2011.11.018

Helmrich, A., M. Ballarino, and L. Tora. 2011. Collisions between replication and transcription complexes cause common fragile site instability at the longest human genes. *Mol. Cell.* 44:966–977. http://dx.doi.org/10.1016/j.molcel.2011.10.013

Kanatsu-Shinohara, M., S. Takashima, and T. Shinohara. 2010. Transmission distortion by loss of p21 or p27 cyclin-dependent kinase inhibitors following competitive spermatogonial transplantation. *Proc. Natl. Acad. Sci. USA.* 107:6210–6215. http://dx.doi.org/10.1073/pnas.0914448107

Kim, N., S.N. Huang, J.S. Williams, Y.C. Li, A.B. Clark, J.E. Cho, T.A. Kunkel, Y. Pommier, and S. Jinks-Robertson. 2011. Mutagenic processing of ribonucleotides in DNA by yeast topoisomerase I. *Science.* 332:1561–1564. http://dx.doi.org/10.1126/science.1205016

Lallemand, Y., V. Luria, R. Haffner-Krausz, and P. Lonai. 1998. Maternally expressed PGK-Cre transgene as a tool for early and uniform activation of the Cre site-specific recombinase. *Transgenic Res.* 7:105–112. http://dx.doi.org/10.1023/A:1008868325009

Lazzaro, F., D. Novarina, F. Amara, D.L. Watt, J.E. Stone, V. Costanzo, P.M. Burgers, T.A. Kunkel, P. Plevani, and M. Muzi-Falconi. 2012. RNase H and postreplication repair protect cells from ribonucleotides incorporated in DNA. *Mol. Cell.* 45:99–110. http://dx.doi.org/10.1016/j.molcel.2011.12.019

Lee-Kirsch, M.A., M. Gong, D. Chowdhury, L. Senenko, K. Engel, Y.A. Lee, U. de Silva, S.L. Bailey, T. Witte, T.J. Vyse, et al. 2007. Mutations in the gene encoding the 3′-5′ DNA exonuclease TREX1 are associated with systemic lupus erythematosus. *Nat. Genet.* 39:1065–1067. http://dx.doi.org/10.1038/ng2091

Morita, M., G. Stamp, P. Robins, A. Dulic, I. Rosewell, G. Hrivnak, G. Daly, T. Lindahl, and D.E. Barnes. 2004. Gene-targeted mice lacking the Trex1 (DNase III) 3′—>5′ DNA exonuclease develop inflammatory myocarditis. *Mol. Cell. Biol.* 24:6719–6727. http://dx.doi.org/10.1128/MCB.24.15.6719-6727.2004

Müller, U., U. Steinhoff, L.F. Reis, S. Hemmi, J. Pavlovic, R.M. Zinkernagel, and M. Aguet. 1994. Functional role of type I and type II interferons in antiviral defense. *Science.* 264:1918–1921. http://dx.doi.org/10.1126/science.8009221

Nick McElhinny, S.A., D. Kumar, A.B. Clark, D.L. Watt, B.E. Watts, E.B. Lundström, E. Johansson, A. Chabes, and T.A. Kunkel. 2010. Genome instability due to ribonucleotide incorporation into DNA. *Nat. Chem. Biol.* 6:774–781. http://dx.doi.org/10.1038/nchembio.424

Reijns, M.A., D. Bubeck, L.C. Gibson, S.C. Graham, G.S. Baillie, E.Y. Jones, and A.P. Jackson. 2011. The structure of the human RNase H2 complex defines key interaction interfaces relevant to enzyme function and human disease. *J. Biol. Chem.* 286:10530–10539. http://dx.doi.org/10.1074/jbc.M110.177394

Reijns, M.A., B. Rabe, R.E. Rigby, P. Mill, K.R. Astell, L.A. Lettice, S. Boyle, A. Leitch, M. Keighren, F. Kilanowski, P.S. Devenney, D. Sexton, G. Grimes, I.J. Holt, R.E. Hill, M.S. Taylor, K.A. Lowson, J.R. Dorin, and A.P. Jackson. 2012. Enzymatic removal of ribonucleotides from DNA is essential for mammalian genome integrity and development. *Cell.* 149:1008–1022. http://dx.doi.org/10.1016/j.cell.2012.04.011.

Rice, G.I., J. Bond, A. Asipu, R.L. Brunette, I.W. Manfield, I.M. Carr, J.C. Fuller, R.M. Jackson, T. Lamb, T.A. Briggs, et al. 2009. Mutations involved in Aicardi-Goutières syndrome implicate SAMHD1 as regulator of the innate immune response. *Nat. Genet.* 41:829–832. http://dx.doi.org/10.1038/ng.373

Rickert, R.C., J. Roes, and K. Rajewsky. 1997. B lymphocyte-specific, Cre-mediated mutagenesis in mice. *Nucleic Acids Res.* 25:1317–1318. http://dx.doi.org/10.1093/nar/25.6.1317

Rodríguez, C.I., F. Buchholz, J. Galloway, R. Sequerra, J. Kasper, R. Ayala, A.F. Stewart, and S.M. Dymecki. 2000. High-efficiency deleter mice show that FLPe is an alternative to Cre-loxP. *Nat. Genet.* 25:139–140. http://dx.doi.org/10.1038/75973

Sekiguchi, J., and S. Shuman. 1997. Site-specific ribonuclease activity of eukaryotic DNA topoisomerase I. *Mol. Cell.* 1:89–97. http://dx.doi.org/10.1016/S1097-2765(00)80010-6

Stetson, D.B., J.S. Ko, T. Heidmann, and R. Medzhitov. 2008. Trex1 prevents cell-intrinsic initiation of autoimmunity. *Cell.* 134:587–598. http://dx.doi.org/10.1016/j.cell.2008.06.032

Stirling, P.C., Y.A. Chan, S.W. Minaker, M.J. Aristizabal, I. Barrett, P. Sipahimalani, M.S. Kobor, and P. Hieter. 2012. R-loop-mediated genome instability in mRNA cleavage and polyadenylation mutants. *Genes Dev.* 26:163–175. http://dx.doi.org/10.1101/gad.179721.111

Testa, G., J. Schaft, F. van der Hoeven, S. Glaser, K. Anastassiadis, Y. Zhang, T. Hermann, W. Stremmel, and A.F. Stewart. 2004. A reliable lacZ expression reporter cassette for multipurpose, knockout-first alleles. *Genesis.* 38:151–158. http://dx.doi.org/10.1002/gene.20012

Turchi, J.J., L. Huang, R.S. Murante, Y. Kim, and R.A. Bambara. 1994. Enzymatic completion of mammalian lagging-strand DNA replication. *Proc. Natl. Acad. Sci. USA.* 91:9803–9807. http://dx.doi.org/10.1073/pnas.91.21.9803

Wahba, L., J.D. Amon, D. Koshland, and M. Vuica-Ross. 2011. RNase H and multiple RNA biogenesis factors cooperate to prevent RNA:DNA hybrids from generating genome instability. *Mol. Cell.* 44:978–988. http://dx.doi.org/10.1016/j.molcel.2011.10.017

Yang, Y.G., T. Lindahl, and D.E. Barnes. 2007. Trex1 exonuclease degrades ssDNA to prevent chronic checkpoint activation and autoimmune disease. *Cell.* 131:873–886. http://dx.doi.org/10.1016/j.cell.2007.10.017